Journal of Alloys and Compounds 509 (2011) 8625–8631

Contents lists available at ScienceDirect

Journal of Alloys and Compounds

journal homepage: www.elsevier.com/locate/jallcom

Effect of precipitates on microstructures and properties of forged Mg–10Gd–2Y–0.5Zn–0.3Zr alloy during ageing process

X.Z. Han, W.C. Xu, D.B. Shan*

School of Materials Science and Engineering, Harbin Institute of Technology, Harbin 150001, Heilongjiang, PR China

ARTICLE INFO

Article history:
Received 16 April 2011
Received in revised form 16 June 2011
Accepted 18 June 2011
Available online 24 June 2011

Keywords:
Metals and alloys
Microstructure
Grain boundaries
Mechanical properties

ABSTRACT

The precipitate behavior during forging and ageing process of Mg–10Gd–2Y–0.5Zn–0.3Zr alloy has been investigated by X-ray diffraction, scanning electron microscopy and transmission electron microscopy. The mechanical properties of the alloy after forging and ageing process have been evaluated using Vickers hardness and room-temperature tensile tests. The results show that precipitation of 14H-type long period stacking order (LPSO) phase is the main strengthening phase in the as-forged alloy. The LPSO phase and refinement of grains contribute to the strength improvement of the alloy after forging process. The optimal mechanical properties of the alloy are obtained when it is aged at 200 °C for 60 h, which mainly owes to the precipitation of large amounts of β′ and 14H-type LPSO phases on the α-Mg matrix. The growth of secondary phases, widening of soft precipitate free zones and coarsening of grains during subsequent ageing process at higher temperature lead to the decrease of mechanical properties of the alloy.

1. Introduction

Today, Magnesium and its alloys are attracting more and more attentions around the world because of the low density, high special strength and good thermal conductivity. The special advantages of Magnesium alloys promise a potential wide use in light-weight components for aerospace and automobile industry. However, the extensive application of magnesium alloys is limited by their poor strength and heat resistance at room and elevated temperature. Rare earth (RE) elements are added into Magnesium alloys to form some secondary phases in order to improve the strength of the alloys. More recently, new developed Magnesium alloys containing some RE elements exhibit better mechanical properties at elevated temperature than WE54 which has the top strength among the existing commercial magnesium alloys [1–3].

The precipitate behavior of main strengthening phases in Magnesium alloys containing rare earth during ageing process has been studied for years and some results have been put forward by many researchers [4–12]. It was reported that the precipitation sequence for binary Mg–Y alloy is: supersaturated solid solution (S.S.S.S.) → β″($D0_{19}$) → β′(cbco) → β($Mg_{24}Y_5$), while that for binary Mg–Gd alloys is: (S.S.S.S.) → β″ → β′ → β(Mg_5Gd) [4,12]. He et al. [5] proposed the precipitation sequence of Mg–10Gd–3Y–0.4Zr during ageing process: super-saturated solid solution (S.S.S.S.) → β″ → β′ → β_1(fcc) → β(fcc), which was confirmed by other researchers [6–9]. The β″ and β′ phases precipitating at the early stage of ageing process are main strengthening phases for Magnesium alloys [6,10]. The metastable β″ phase has a $D0_{19}$ crystal structure (hexagonal, $a = 0.642$ nm, $c = 0.521$ nm) and intermediate β′ phase has a base-centered orthorhombic structure ($a = 0.640$ nm, $b = 2.223$ nm, $c = 0.521$ nm). The β″ transforms to β′ phase quickly during subsequent ageing process [11,12]. In 2001, a novel $Mg_{97}Zn_1Y_2$ alloy containing long period stacking order (LPSO) phase was developed and exhibited excellent mechanical properties with the yield strength of 610 MPa and the elongation of 5% [13,14]. Gao et al. demonstrated that the novel LPSO phase in Mg–10Y–5Gd–2Zn–0.5Zr alloy is constructed by ABCBCB (6H-type) stacking of closed-packed planes of Magnesium crystalline [15]. Honma et al. [16] and Liu et al. [17] found that 14H-LPSO phase has an important effect on the ultimate tensile strength of Mg–5Y–4Gd–*x*Zn–0.4Zr and Mg–1.2Y–2.0Gd–*x*Zn–0.2Zr alloys. The combination effect of coherent LPSO phase and refinement of α-Mg grains contribute to a high tensile yield strength and large elongation of warm-extruded Mg–Zn–Gd alloy [18].

Forging process plays an important role in the formation of complex-shaped components with high strength in aviation and aerospace industries. Nevertheless, the microstructure evolution and precipitate behavior in as-forged Magnesium alloy with rare earth elements have seldom been studied until now. The strengthening mechanism of Magnesium alloy during forging and subsequent ageing process is not clear yet and systematic study is needed to give more details about these issues. In the present

* Corresponding author. Tel.: +86 451 86418732; fax: +86 451 86418732.
E-mail address: shandb@hit.edu.cn (D.B. Shan).

0925-8388/$ – see front matter © 2011 Elsevier B.V. All rights reserved.
doi:10.1016/j.jallcom.2011.06.086

study, Mg–10Gd–2Y–0.5Zn–0.3Zr alloy, a typical age-hardening Magnesium alloy, was submitted forging and ageing process. The precipitate behavior and microstructure evolution during forging and ageing process were investigated by SEM and TEM observation. The high strength and adequate elongation of the alloy were achieved through optimizing heat treatment parameters. The relationship between microstructures and mechanical properties of the alloy was also discussed in detail.

2. Experimental procedure

The nominal composition of Magnesium alloy used in this investigation was Mg–10Gd–2Y–0.5Zn–0.3Zr (at.% nominal composition), which was prepared from high purity Mg (99.95%), Zn (99.9%), Mg–20Y, Mg–30.6Gd and Mg–30.33Zr (wt%) master alloys in an electric resistance furnace at about 750 °C under a mixed gas atmosphere of SF_6 and CO_2. The ingots were homogenized at 510 °C for 10 h followed by quenching into hot water at 80 °C, and then forging process was carried out at 470 °C. The specimens for tensile test, Vickers hardness test and ageing process were machined from the forged block of 200 mm width, 300 mm length and 200 mm thickness. Artificial ageing process was carried out at 200 °C, 225 °C and 250 °C with different time length in an ageing furnace.

The mechanical properties of the aged specimens were measured on an INSTRON5559 tensile testing machine with crosshead speed of 1 mm/min. Rods for tensile test are of 3 mm gauge diameter and 15 mm gauge length. Vickers hardness test was performed by a Vickers hardness tester under a load of 300 N and holding time of 30 s. Specimens for optical microscopy (OM) were prepared by a conventional mechanical polishing technique. The specimens were etched in a solution of 4 vol.% nital and the microstructure was analyzed by OM and scanning electron microscope (SEM) equipped with an energy dispersive X-ray spectrometer (EDS). The characterization of phases was performed by X-ray diffraction (XRD) and TECNI-2010 transmission electron microscopy (TEM) operating at 300 kV. The thin foils for TEM were prepared by ion polishing system.

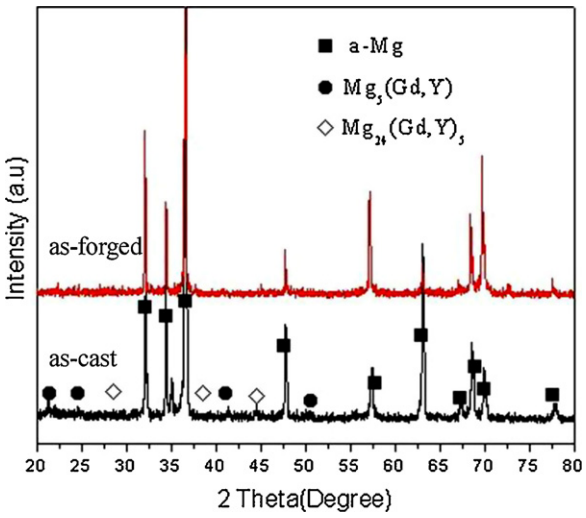

Fig. 1. XRD patterns of as-cast and as-forged alloys.

3. Results

3.1. As-cast and as-forged microstructures

Fig. 1 shows the XRD patterns of as-cast and as-forged alloys. The phase composition of as-cast alloy is: α-Mg solid solution, $Mg_{24}(Gd,Y)_5$ and $Mg_5(Gd,Y)$ phases. Fig. 2 shows the microstructures of as-cast and as-forged alloys. It shows that a number of

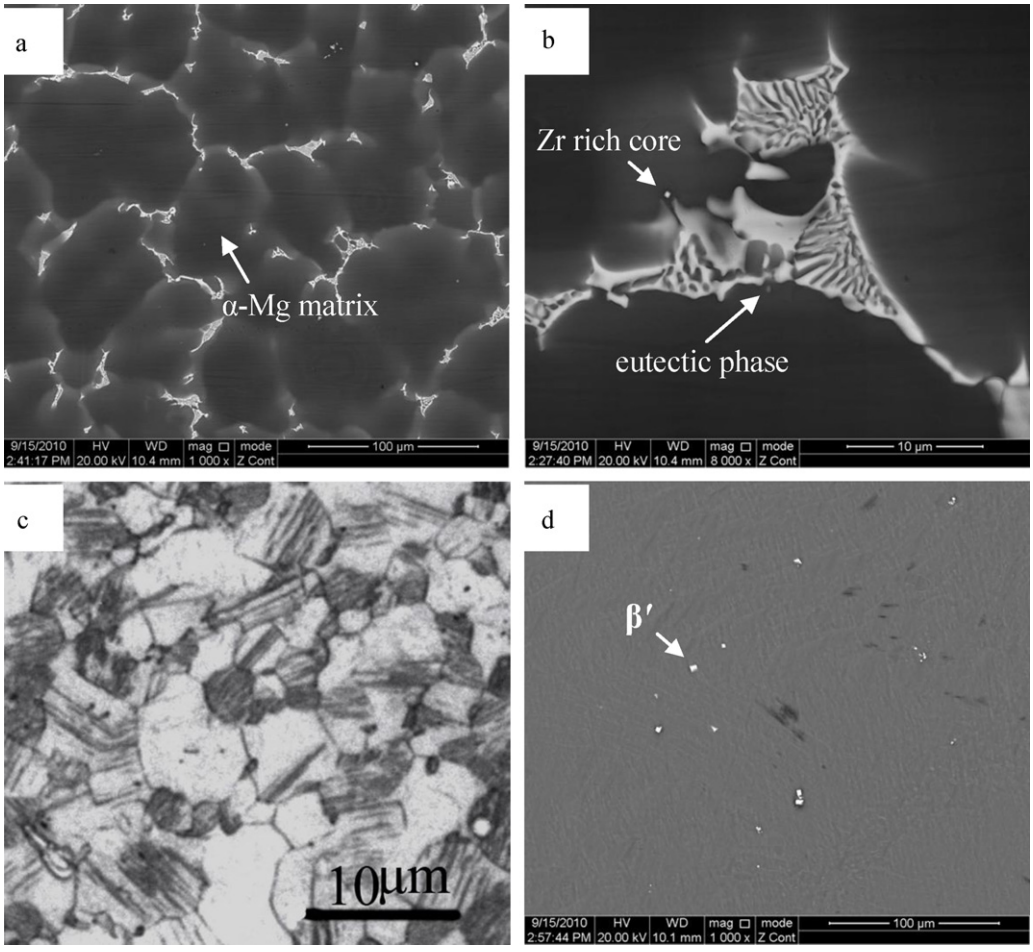

Fig. 2. SEM image and OM microstructure of as-cast and as-forged alloy, (a) SEM image of as-cast alloy, (b) large magnification of (a). (c) OM microstructure of as-forged alloy, (d) SEM image of as-forged alloy.

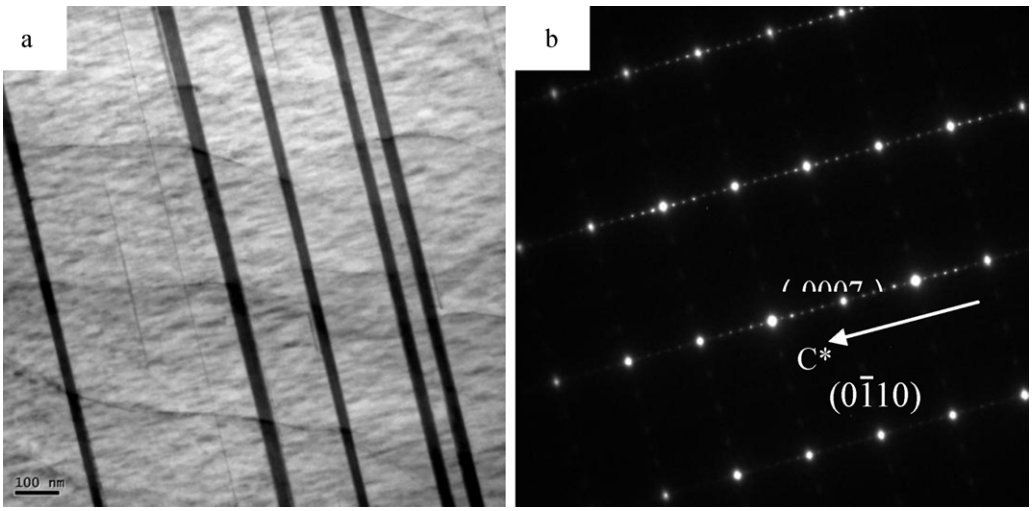

Fig. 3. TEM image and corresponding selected area electron diffraction (SAED) pattern of lamellar phase in the as-forged alloy, (a) TEM bright image and (b) SAED pattern of lamellar phase in (a). Electron beam is parallel to $[2\ \bar{1}\ \bar{1}\ 0]_{\alpha}$.

dendrites locate at the triple points of α-Mg grains and distribute along the grain boundaries discontinuously in the as-cast alloy. Some tiny and round Zr-rich particles also distribute on the α-Mg matrix, as shown in Fig. 2(a) and (b). Nevertheless, the grain size becomes smaller and some new cuboid phases (β′ phase) distribute at the grain boundaries or within grains after forging process compared to that of as-cast alloy, as shown in Fig. 2(c) and (d). Furthermore, large amounts of lamellas parallel to each other precipitate within grains. The average grain size is about 8 μm after forging process.

Fig. 3 shows the TEM image and selected area electron diffraction (SAED) pattern taken from lamellar region in the as-forged alloy. Many lamellas are seen to precipitate on the matrix after forging process, as shown in Fig. 3(a). SAED pattern shows that there are seven extra diffraction spots at the position of $n/7(0\,0\,0\,1)_{hcp}$, which suggests that the lamellar phase is 14H-type LPSO phase with a 14 basal-plane periodicity, as shown in Fig. 3(b). Here, it should be pointed out that no eutectic compounds and just small amounts of $Mg_5(Gd,Y)$ phase distribute on the matrix according to TEM observation, which is different from that of as-cast alloy.

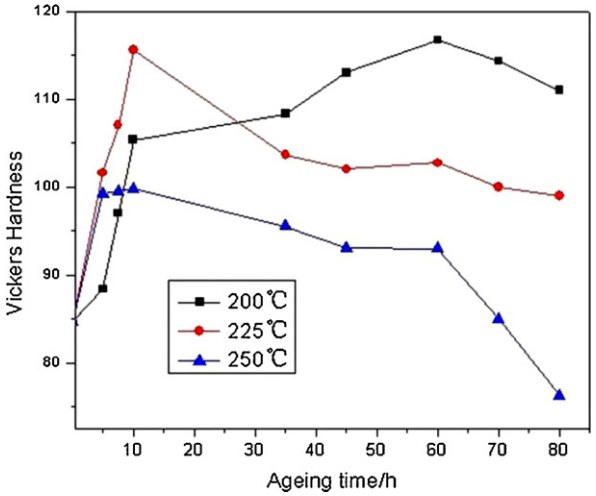

Fig. 4. Age hardening behavior of as-forged alloy at 200 °C, 225 °C and 250 °C.

3.2. Ageing hardening behavior of as-forged alloy

Fig. 4 shows ageing hardening response of as-forged alloy at 200 °C, 225 °C and 250 °C with different ageing time. During ageing process at 200 °C, the hardness of the as-forged alloy increases obviously until 10 h and then slowly reaches the peak hardness of 116 VHN at 60 h. Nevertheless, the ageing time to peak hardness of the as-forged alloy aged at 225 °C and 250 °C decreases to 10 h and 5 h which corresponds to peak hardness of 114 VHN and 99 VHN, respectively. The obtainment of peak hardness of the alloy involves the formation of secondary phases and the formation rate controlled by diffusion of solute atoms [19]. Increasing temperature can accelerate diffusion rate of RE elements in the alloy and more secondary strengthening phases can be formed during ageing process, which leads to the varied peak hardness with different ageing temperature. The hardness after peak value decreases gradually with increasing ageing time, which results from coarsening of secondary phases and α-Mg grains.

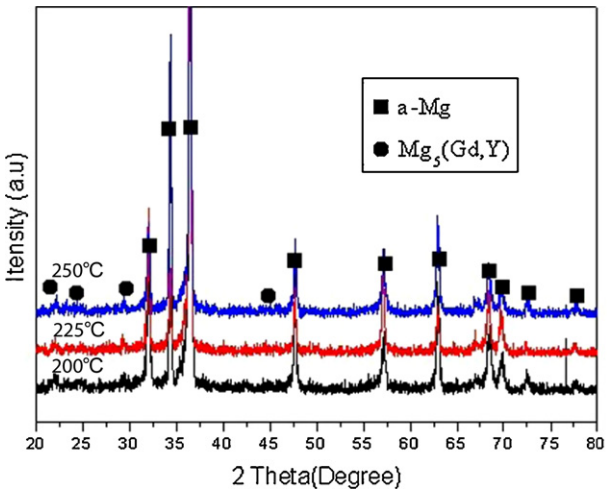

Fig. 5. XRD patterns of peak-aged alloys at 200 °C, 225 °C and 250 °C.

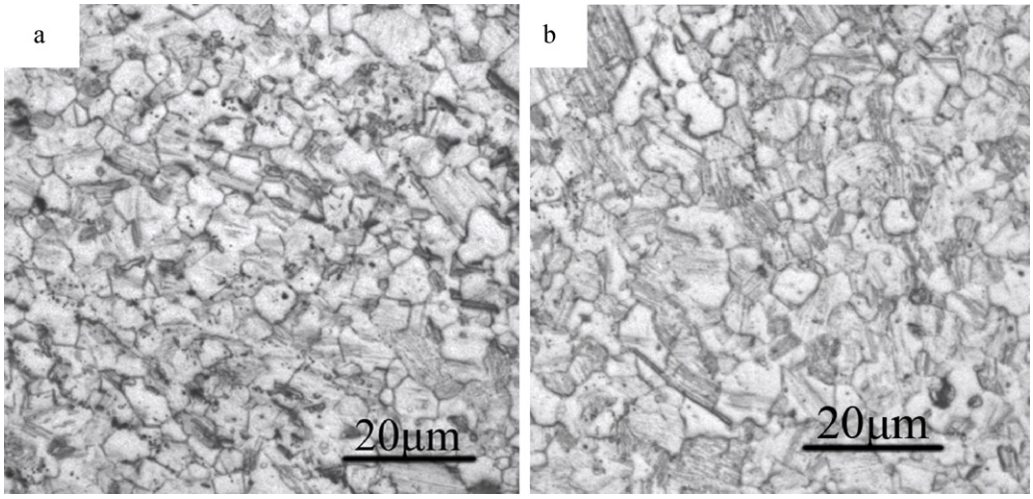

Fig. 6. OM microstructures of peak-aged alloy at: (a) 200 °C, (b) 225 °C.

3.3. Precipitate behavior of peak-aged alloy

Fig. 5 shows XRD patterns of peak-aged alloy at 200 °C, 225 °C and 250 °C. The phase composition of the alloys aged at 200 °C, 225 °C and 250 °C are similar to each other. Only two phases designated as α-Mg and $Mg_5(Gd,Y)$ can be recognized from the results. Fig. 6 presents the OM microstructures of peak-aged alloy at 200 °C and 225 °C. It suggests that many tiny particles locate at both grain boundaries and within grains in the peak-aged alloy at 200 °C. The average grain size is about 11 μm in the peak-aged alloy at 200 °C, which is slightly larger than that of as-forged specimens, as shown in Fig. 6(a). Fig. 6(b) indicates that the grains become coarse and the particles located at the grain boundaries decrease with increasing ageing temperature. Average grain size in the peak-aged alloy at 225 °C is 13 μm and also the microstructure is not uniform compared to that of peak-aged alloy at 200 °C.

Fig. 7 shows the TEM images and corresponding SAED patterns of β′ phase with the aim to investigate the precipitate behavior of β′ phase during ageing process. Densities of precipitates are observed on the matrix in the peak-aged alloy at 200 °C, indicated by arrows in Fig. 7(a). These tiny precipitates distribute uniformly on the matrix and corresponding SAED patterns confirms the precipitation of β′ phase with base-centered orthorhombic crystal structure, shown in Fig. 7(b). It is found that β′ phase with the shape of convex lens viewed from $[0\,0\,0\,1]_\alpha$ direction precipitates along $\{1\,1\,\bar{2}\,0\}_\alpha$ through carefully analyzing the distribution of β′ phase on the matrix, as shown in Fig. 7(b) and (f). Corresponding SAED patterns show some extra diffraction spots in $1/4[0\,1\,\bar{1}\,0]_\alpha$, $1/2[0\,1\,\bar{1}\,0]_\alpha$ and $3/4[0\,1\,\bar{1}\,0]$ Mg reflections, as shown in Fig. 7(c) and (d), which suggests that the crystal parameters of β′ phase are: $a = 0.640$ nm, $b = 2.223$ nm, $c = 0.521$ nm [10]. Some clusters of diffraction spots appear between central point and $[0\,1\,\bar{1}\,0]_\alpha$ which confirms three variants of β′ phase around $[0\,0\,0\,1]_\alpha$ zone. The orientation relationship is $[0\,0\,0\,1]_\alpha//[0\,0\,0\,1]_{\beta'}$ and $[2\,\bar{1}\,\bar{1}\,0]_\alpha//(1\,0\,0)_{\beta'}$.

Fig. 8 shows the LPSO phase in the peak-aged alloy at 200 °C. It indicates a high density of fine lamellar phases parallel to each other precipitate on the matrix. Corresponding fast Fourier transformation indicates seven extra diffraction spots between central point and $(0\,0\,0\,1)_\alpha$ and even the distance between two lamellas is equal to ~1.76 nm, which is similar to 1.80 nm of 14H-type LPSO phase [20]. It suggests this LPSO phase is stable during subsequent ageing process, which mainly contributes to the high strength of Mg–10Gd–2Y–0.5Zn–0.3Zr at elevated temperature.

Table 1
Mechanical properties of Mg–10Gd–2Y–0.5Zn–0.3Zr alloy.

State	YTS (MPa)	UTS (MPa)	HV	Elongation (%)
As-cast	114	162	80	4.2
As-forged	210	308	87	7.5
T5, 200 °C-60 h	273	406	116	5.9
T5, 225 °C-10 h	248	362	114	5.7
T5, 250 °C-10 h	253	356	99	4.05

3.4. Mechanical properties of the aged alloy

The mechanical properties of as-cast, as-forged and peak-aged alloy at different temperature are shown in Table 1. It indicates forging process has an obvious effect on the improvement of the mechanical properties of the alloy, which results from the precipitation of the 14H-type LPSO phase and refinement of α-grains. The ultimate tensile strength (UTS) of the alloy aged at 200 °C, 60 h reaches the peak value with UTS and adequate elongation of 406 MPa and 5.9%, respectively. However, the peak strength of the alloy decreases quickly with increasing ageing temperature.

4. Discussion

Generally, the Mg–10Gd–2Y–0.5Zn–0.3Zr alloy investigated in present paper shows high strength after forging and ageing process. Based on the microstructure evolution analysis, it can be seen that the precipitation of β′ and 14H-type LPSO phases has an obvious effect on the mechanical properties of the alloy. The high strength of the as-forged alloy is attributed to the formation of β′ phase, 14H-type LPSO phase and refinement of α-Mg grains after forging process. More β′ and 14H-type LPSO phases precipitate from α-Mg matrix during ageing process at 200 °C while no β″ phase is found in the aged alloy because of longer ageing time [6,7]. The peak strength of the aged alloy at 200 °C is achieved when the volume fraction of the 14-type LPSO and β′ phase becomes the largest on the matrix. Fig. 9 shows the TEM image of the 14-type LPSO phase inhibiting dislocation sliding. It can be seen that dislocation sliding becomes more difficult with the increase of the 14-type LPSO phase on the matrix. The effect of long and linear LPSO phase in inhibiting sliding of dislocation is more obvious than β′ phase with convex lens shape.

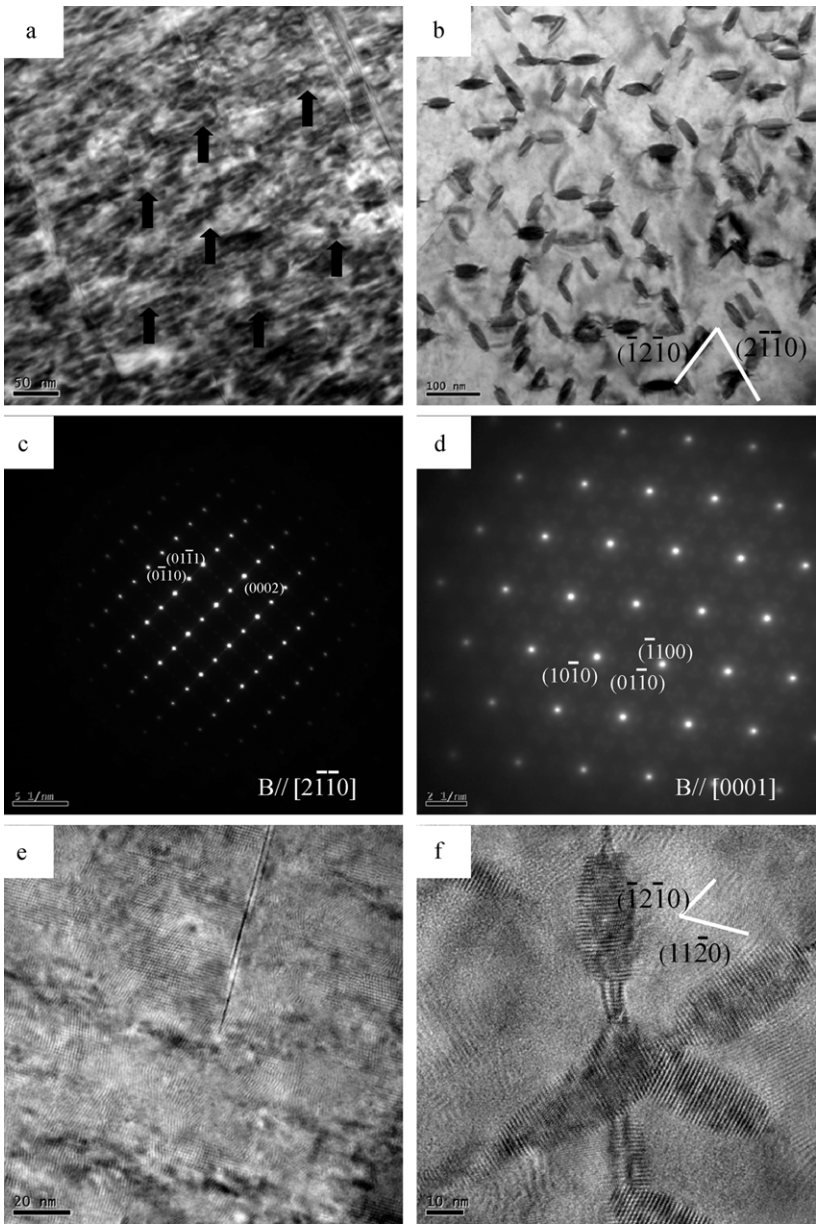

Fig. 7. TEM images, corresponding SAED patterns and high-resolution TEM images of β′ phase during ageing process at 200 °C and 250 °C, (a) and (b) TEM bright field images viewed from $[2\ \bar{1}\ \bar{1}\ 0]_\alpha$ and $[0\,0\,0\,1]_\alpha$, (c) and (d) corresponding SAED patterns of β′ phase in (a) and (b), (e) and (f) high-resolution TEM images of β′ phase in (a) and (b).

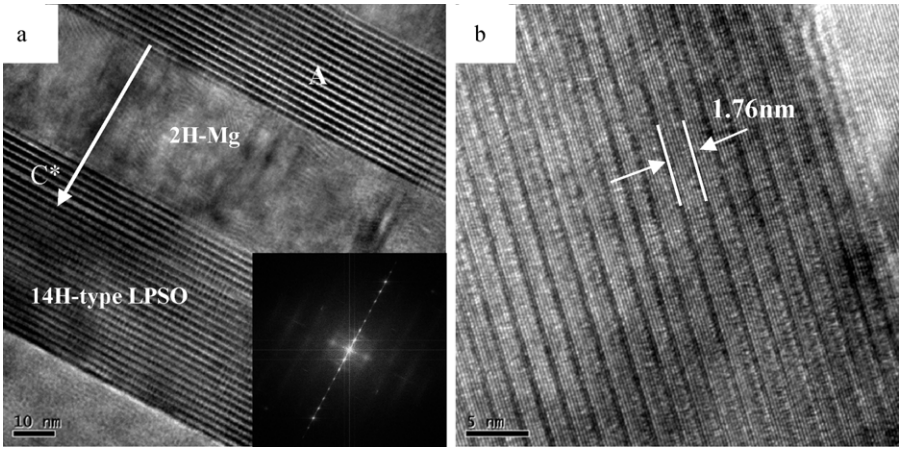

Fig. 8. High resolution TEM image of 14H-type LPSO phase in the peak-aged alloy at 200 °C, (a) TEM image of 14H-type LPSO phase, (b) large magnitude of point A in (a), corresponding fast Fourier transformation inserted in (a).

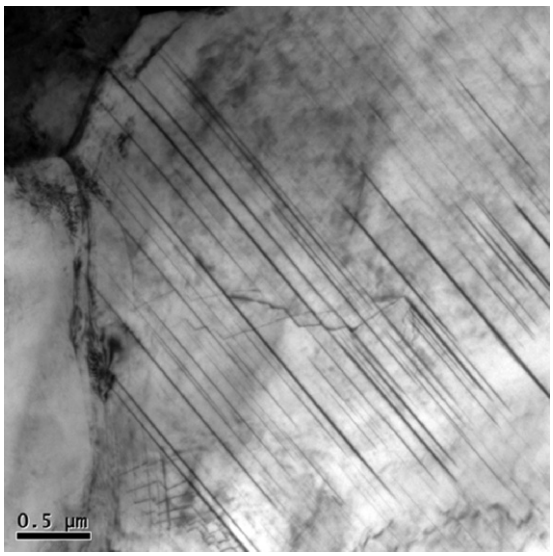

Fig. 9. TEM image of dislocation sliding through 14H-type LPSO phases of alloy aged at 200 °C, 60 h.

Thus, the peak strength of the aged alloy at 200 °C mainly results from the precipitation of 14-type LPSO phase which can inhibit sliding of dislocations and growth of grain boundaries. With ageing temperature increasing, coarsening of grains and secondary phases results in the inferior mechanical properties of the alloy after ageing process.

Grain boundary structure is an important factor affecting the mechanical properties of Magnesium alloys [21–23]. The evolution of grain boundary structure is accompanied by two coinstantaneous procedures: growing of precipitates at grain boundary and widening of precipitates free zones (PFZ) [10]. The metastable phase dissolves into the matrix in order to lower energy and solute atoms disperse to the grain boundaries with formation of the soft PFZ. Fig. 10 presents the precipitates evolution at grain boundary during ageing process. Many secondary phases precipitate at grain boundaries in peak-aged alloy at 200 °C and the PFZ becomes obvious at the same time. Further ageing process at 250 °C promotes the growing of precipitates at grain boundaries and widening of the soft PFZ, as shown in Fig. 10(a) and (b). Many diffraction spots of low brightness from grain boundary precipitates and energy dispersive X-ray spectrometer analysis, as shown in Fig. 10(c) and (d), confirm that the precipitates at grain boundaries are β′ phases. It can be deduced that, accompanied by wider PFZ, more β′ phases transform to the stable β phase with ageing time increasing at 250 °C, which deteriorates mechanical properties of the alloy during ageing process. Therefore, the widening of soft precipitate free zone,

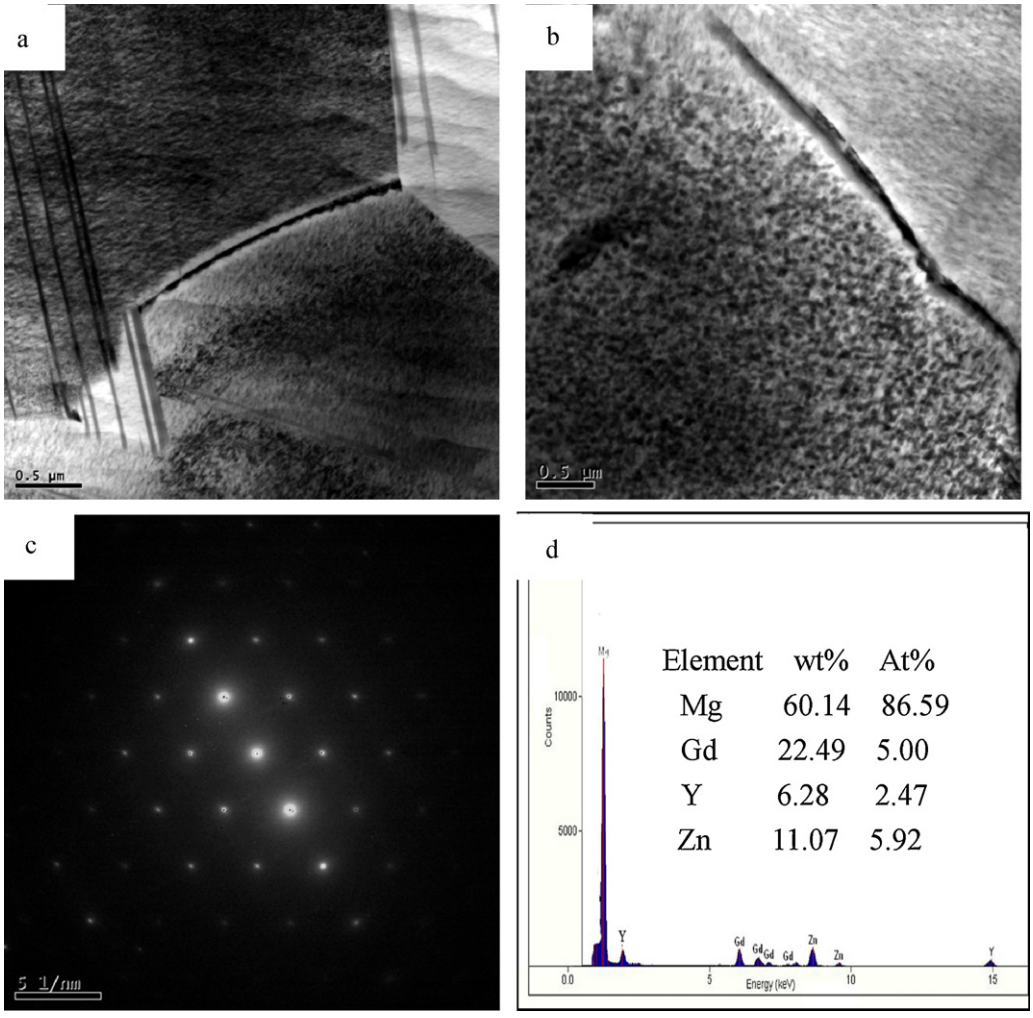

Fig. 10. TEM images of grain boundaries in the peak-aged alloy, corresponding SAED pattern and EDS analysis of precipitates at grain boundaries, (a) 200 °C, 60 h (b) 250 °C, 10 h. (c) Corresponding SAED pattern of precipitates at grain boundary in (a). (d) EDS analysis of precipitates at grain boundary in (b).

growth of secondary phases and grains cause the poor mechanical properties after ageing process.

5. Conclusion

In the present paper, the precipitates behavior during forging and ageing process has been investigated. The strength increment of the as-forged Mg–10Gd–2Y–0.5Zn–0.3Zr alloy mainly results from precipitating of 14H-type LPSO phase and grain refinement during forging process. Many β′ and 14H-type LPSO phases distribute on the α-Mg matrix at the early stage of ageing process. The β′ phase precipitates along $\{1\,1\,\bar{2}\,0\}_\alpha$ with three variants in the matrix. With ageing time increasing at 200 °C, amounts of β′ and 14H-type LPSO phases precipitate on the α-Mg matrix until 60 h. The optimal mechanical properties are obtained in the alloy aged at 200 °C for 60 h with the UTS of 406 MPa and adequate elongation of 5.9%. Strengthening mechanism of the aged alloy is controlled by the precipitation of β′ and 14H-type LPSO phases which can inhibit sliding of dislocations and growth of grain boundaries. The growth of secondary phases and grains, widening of soft precipitates free zones lead to the poor mechanical properties of the alloy after ageing process at elevated temperature.

Acknowledgement

This work is supported by The National Natural Science Foundation of China (no. 50775051).

References

[1] L.L. Rokhlin, Proceedings of NATO Advanced Study Institute, Kluwer, 1998, p. 443.
[2] S. Kamado, Y. Kojima, R. Ninomiya, K. Kubota, in: G.W. Lorimer (Ed.), Proceedings of the Third International Magnesium Conference, Institute of Materials, Manchester, UK, 1997, p. 327.
[3] I. Anthony, S. Kamado, Y. Kojima, Mater. Trans. 42 (2001) 1212.
[4] B. Smola, I. Stulˇıkovaˇı, F. von Buch, B.L. Mordike, Mater. Sci. Eng. A 324 (2002) 113.
[5] S.M. He, X.Q. Zeng, L.M. Peng, X. Gao, J.F. Nie, W.J. Ding, J. Alloys Compd. 421 (2006) 309–313.
[6] K. Liu, J.H. Zhang, D.X. Tang, L.L. Rokhlin, F.M. Elkinc, J. Meng, Mater. Chem. Phys. 117 (2009) 107–112.
[7] K. Liu, L.L. Rokhlin, F.M. Elkinc, D.X. Tang, J. Meng, Mater. Sci. Eng. A 527 (2010) 828–834.
[8] S.Q. Liang, D.K. Guan, L. Chen, Z.H. Gao, H.X. Tang, X.T. Tong, R. Xiao, Mater. Des. 32 (2011) 361–364.
[9] S.M. He, X.Q. Zeng, L.M. Peng, X. Gao, J.F. Nie, W.J. Ding, J. Alloys Compd. 427 (2007) 316–323.
[10] K.Y. Zheng, J. Dong, X.Q. Zeng, W.J. Ding, Mater. Sci. Eng. A 489 (2008) 44–54.
[11] H. Karimzadeh, Ph.D. Thesis, University of Manchester, U.K. (1985).
[12] G.W. Lorimer, in: C. Baker, G.W. Lorimer, W. Unsworth (Eds.), Proceedings of the London Conference on Magnesium Technology, The Institute of Metals, London, U.K., 1986, p. 47.
[13] Y. Awamura, K. Hayashi, A. Inoue, T. Masumoto, Mater. Trans. 42 (2001) 1172.
[14] A. Noue, Y. Kawamura, M. Matsusita, K. Hayashi, J. Koike, J. Mater. Res. Soc. 16 (2001) 1894.
[15] Y. Gao, Q.D. Wang, J.H. Gu, Y. Zhao, Y. Tong, D.D. Yin, J. Alloys Compd. 477 (2009) 374–378.
[16] T. Honma, T. Ohkubo, S. Kamado, K. Hono, Acta Mater. 55 (2007) 4137–4150.
[17] K. Liu, J.H. Zhang, G.H. Su, D.X. Tang, L.L. Rokhlin, F.M. Elkin, J. Meng, J. Alloys Compd. 481 (2009) 811–818.
[18] M. Yamasaki, T. Anan, S. Yoshimoto, Y. Kawamur, Scripta Mater. 53 (2005) 799–803.
[19] E. Abe, Y. Kawamura, K. Hayashi, A. Inoue, Acta Mater. 50 (2002) 3845.
[20] Y.M. Zhu, A.J. Morton, J.F. Nie, Acta Mater. 58 (2010) 2936–2947.
[21] G. Lutjeringa, J. Albrecht, C. Sauer, T. Krull, Mater. Sci. Eng. A 468–470 (2007) 201–209.
[22] S.P. Lynch, Mater. Sci. Eng. A 136 (1991) 25–43.
[23] S. Kuramoto, G. Itoh, M. Kanno, Met. Mater. Trans. A 27 (1996) 3081–3088.